Chem Soc Rev

TUTORIAL REVIEW

View Article Online
View Journal | View Issue

Cite this: *Chem. Soc. Rev.*, 2015, 44, 8399

Dielectric shell isolated and graphene shell isolated nanoparticle enhanced Raman spectroscopies and their applications

Jian-Feng Li,*[a] Jason R. Anema,*[b] Thomas Wandlowski[c] and Zhong-Qun Tian[a]

Received 28th June 2015

DOI: 10.1039/c5cs00501a

www.rsc.org/chemsocrev

Surface-enhanced Raman scattering (SERS) is a powerful technique that provides fingerprint vibrational information with ultrahigh sensitivity. However, only a few metals (gold, silver and copper) yield a large SERS effect, and they must be rough at the nanoscale. Shell-isolated nanoparticle-enhanced Raman spectroscopy (SHINERS) was developed to overcome the long-standing materials and morphological limitations of SERS. It has already been applied in a variety of fields such as materials science, electrochemistry, surface science, catalysis, food safety and the life sciences. Here, the principles and applications of SHINERS are highlighted. To provide an understanding of the plasmonics involved, finite-difference time-domain (FDTD) calculations and single nanoparticle SHINERS experiments are reviewed. Next, various shell-isolated nanoparticle (SHIN) types are described. Then a number of applications are discussed. In the first application, SHINERS is used to characterize the adsorption processes of pyridine on Au(*hkl*) single-crystal electrode surfaces. Then, SHINERS' applicability to food inspection and cultural heritage science is demonstrated by the detection of parathion and fenthion pesticides, and Lauth's violet (thionine dye). Finally, graphene-isolated Au nanoparticles (GIANs) are shown to be effective for multimodal cell imaging, photothermal cancer therapy and photothermally-enhanced chemotherapy. SHINERS is a fast, simple and reliable method, suitable for application to many areas of science and technology. The concept of shell-isolation can also be applied to other surface-enhanced spectroscopies such as fluorescence, infrared absorption and sum frequency generation.

Key learning points

(1) In SHINERS, the gold nanoparticle core acts as a Raman signal amplifier. The ultrathin shell allows enhanced electromagnetic field from the surface of the core to extend past the surface of the shell and probe the nanoparticle's chemical environment; yet the shell is pinhole-free and it therefore prevents the interaction of the core with any components of the chemical environment.

(2) SHINERS enhancement deceases rapidly with increasing shell thickness, but the preparation of an ultrathin (less than 5 nm) shell is possible for a variety of nanoparticle types.

(3) Gold@silica SHINERS nanoparticles can be used to fully characterize monolayer adsorption on atomically flat single-crystal surfaces, which have traditionally been excluded from SERS investigation.

(4) SHINERS is a convenient method that can be applied to food inspection and cultural heritage science. An appropriately chosen shell can eliminate metal–molecule interactions which cause an analyte's SERS spectrum to differ from its ordinary Raman spectrum, thus allowing comparison with ordinary Raman spectra in the literature or a library.

(5) Gold@graphene SHINERS nanoparticles have proven effective in multimodal cell imaging and cancer therapy because of their biocompatibility, spectroscopic properties, photothermal properties, and the avenues available for their functionalization.

[a] *MOE Key Laboratory of Spectrochemical Analysis and Instrumentation, State Key Laboratory of Physical Chemistry of Solid Surfaces, and College of Chemistry and Chemical Engineering, Xiamen University, Xiamen, 361005, China. E-mail: li@xmu.edu.cn; Tel: +86-529-218-6192*

[b] *Canadian Conservation Institute, 1030 Innes Road, Ottawa, Ontario, Canada K1B 4S7. E-mail: jason.anema@pch.gc.ca; Tel: +1-613-998-3721*

[c] *Department of Chemistry and Biochemistry, University of Bern, Freiestrasse 3, Bern, CH-3012, Switzerland*

1. Introduction to the shell-isolated mode

In surface-enhanced Raman scattering (SERS),[1–5] Raman signals are enhanced by up to ~10 orders of magnitude[4,6,7] because of a molecule's proximity to a nanostructured, free-electron metal surface. When light of a resonant wavelength is incident upon

this type of surface, it will initiate collective oscillations in electron density called surface plasmons that give narrow regions of enhanced electromagnetic field strength.[8–12] This extremely powerful vibrational spectroscopy can be used to characterize adsorption with single-molecule sensitivity, and hundreds of articles are being published on it each year.[13–15]

To date, SERS has not been adopted as a general tool because of the specific materials and morphologies required. Only a few metals, namely gold, silver and copper, provide a large SERS effect. Furthermore, the signal enhancement provided by the metal nanostructures depends critically on their size, shape and spacing.[8,16] These conditions have limited the breadth of practical applications of SERS in fields where such materials and morphologies are rarely found. For example, the atomically flat surfaces of various single-crystals, which are encountered in surface science and semiconductor technologies, have been almost completely excluded from investigation by SERS.

Traditionally, the SERS substrate has played a dual role as a signal amplifier and as a support for the experiment. We call this approach the "contact mode" (Fig. 1a), and it is from this experimental design that the materials and morphological specificity comes. Since the substrate must be SERS-active, and the support is the same as the substrate, a rather limited variety of supports are available for experimentation.

Tip-enhanced Raman spectroscopy (TERS)[17,18] was introduced in 2000. This technique employs a "non-contact mode" in which the signal amplifier is separated from the surface of interest (Fig. 1b). Here, a sharp gold or a silver tip is excited with a suitable laser and brought within a few nanometers of the sample. The enhanced electromagnetic field generated at the tip extends to the surface of interest, and Raman signals from any support – regardless of material and morphology – can be improved by this field.[18] The Raman signal obtained from a sample in close proximity to a single tip is quite weak, however, and TERS studies usually involve highly Raman-active molecules. Furthermore, the application of TERS to an electrochemical system requires the tip be immersed in solution. Scattering of light at the air–solution interface further reduces signal strength, and the adsorption of solution species on the tip can give misleading information.

Jian-Feng Li

Jian-Feng Li is a Professor of Chemistry at Xiamen University. He received a BSc degree in chemistry from Zhejiang University, and a PhD degree in chemistry from Xiamen University. Professor Li is the principal inventor of SHINERS. His research interests include surface-enhanced Raman spectroscopy, core–shell nanostuctures, surface plasmon resonance, electrochemistry and surface catalysis.

Jason R. Anema

Jason Anema is a Conservation Scientist at the Canadian Conservation Institute (CCI) where he specializes in the materials analysis of heritage objects. He has a BSc degree in chemistry from the University of Manitoba and a PhD degree in chemistry from the University of Victoria. He has been involved with the development of SHINERS-based methods since 2009, first at Xiamen University and then at the CCI.

Thomas Wandlowski is a professor at the University of Bern. He received his Diploma and PhD in physical chemistry from the University of Halle. Professor Wandlowski's research interests include single-crystal electrochemistry, spectro-electrochemistry and single-molecule electronics.

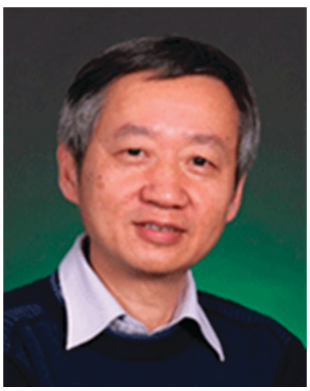

Zhong-Qun Tian

Zhong-Qun Tian is a professor at Xiamen University and serves as a director of the State Key Laboratory of Physical Chemistry of Solid Surfaces. He obtained his BSc at Xiamen University, and his PhD under the supervision of Professor Martin Fleischmann at the University of Southampton. Professor Tian is a Member of the Chinese Academy of Sciences and an advisory board member for more than ten international journals. His main research interests include surface-enhanced Raman spectroscopy, spectro-electrochemistry, nano-electrochemistry and nanomaterials.

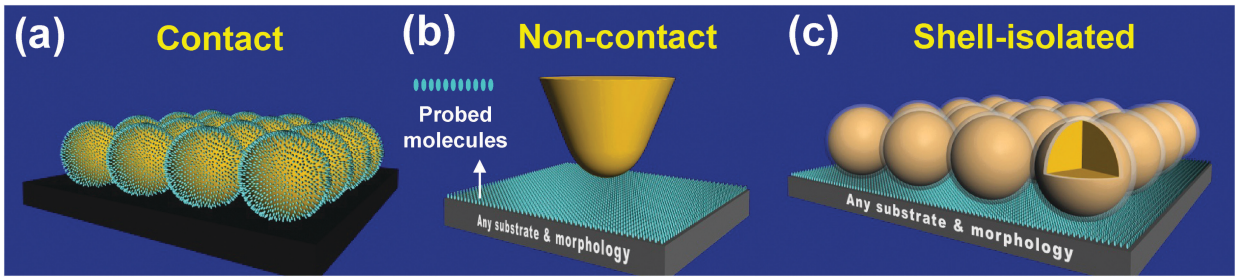

Fig. 1 The working modes of SERS, TERS and SHINERS: the bare gold NPs contact mode (a), the TERS non-contact mode (b), and the SHINERS shell-isolated mode (c). Reprinted with permission from *Nature*, 2010, **464**, 392; copyright 2010 Nature Publishing Group.

In 2010 we reported a new "shell-isolated mode"[19] that, to a large extent, can overcome the problems described above (Fig. 1c). In this approach, the tip is replaced by a film of gold-core silica-shell nanoparticles (Au@SiO_2 NPs). Since each gold core acts as a tip, the equivalent of hundreds or even thousands of tips are excited in the laser spot at the same time. The chemically inert dielectric shell prevents the interaction between the gold core and the system under study. It prevents some molecules from adsorbing on the signal amplifier (those that do not adsorb on silica), and it prevents the gold core from contaminating the system under study. We call this new technique "shell-isolated nanoparticle-enhanced Raman spectroscopy" or "SHINERS",[19–21] and it has already been applied to many challenging systems.[19–30] It has been used to probe structure and processes on materials of different composition and morphology, from metal single-crystals to semiconductors and from food samples to living cells.

Since the introduction of our Au@SiO_2 NPs in 2010, many other structures with a plasmonically-active core and an ultrathin shell have been prepared. Of special interest are those with a noble metal core and a graphene shell.[31,32] It has been shown that such NPs are suitable for multimodal cell imaging and cancer therapy because of their biocompatibility, spectroscopic properties, photothermal properties, and the ways in which they can be functionalized.[32]

2. Advantages of the shell-isolated mode over the contact mode

SHINERS has changed the working mode from direct contact (SERS) or non-contact (TERS) to a shell-isolated one. It has broken some long-standing limitations by allowing the characterization of chemical systems that involve previously inaccessible surface materials and surface morphologies, and it has simplified analysis in challenging environments such as biological systems.

The use of an ultrathin, chemically and electrically inert shell around the NPs can solve numerous problems. It can prevent contact with the chemical environment, contact with the surface of interest, and contact with probe molecules. It can also keep the NPs from aggregating.

(i) Contact with the chemical environment. Bare NPs are unsuitable for use in liquid environments (*e.g.*, in biology and electrochemistry) or gaseous environments (*e.g.*, in catalysis) that contain species which adsorb on the surface (Fig. 2a). Even if a liquid or a gaseous environment does not contain any such adsorbates, probe molecules can move from the surface of interest to the surface of the bare NPs. The SERS signal from molecules adsorbed on the bare NPs, which is likely to be dominant, may interfere with the SERS signal from molecules adsorbed on the surface of interest.

(ii) Electrical contact with the surface. If bare NPs are used in the examination of other metal or semiconductor surfaces, with the bare NPs in direct contact with the surface of interest, charge transfer can significantly affect the electronic structure of the system under study (Fig. 2b).

As an example, SERS and SHINERS spectra showing CO adsorption on Pt(111) are compared in Fig. 3. Two strong bands can be seen in the spectrum obtained with bare gold NPs, one at 2060 cm^{-1} that is due to C–O(Pt) stretching and another at 2125 cm^{-1} that is due to C–O(Au) stretching. The latter is clearly undesirable as it could mislead the interpretation of the spectrum.

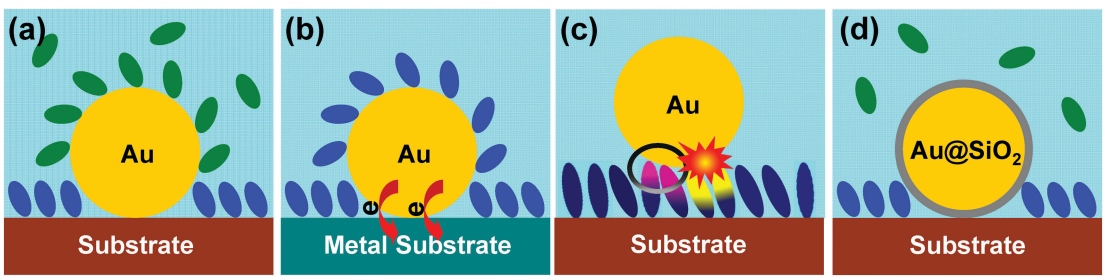

Fig. 2 Schematic illustrations of four different experiments. (a) Contact with the chemical environment may lead to the adsorption of nearby molecules. (b) Electrical contact with the surface may lead to charge transfer. (c) Contact with probe molecules may lead to spectral changes or photocatalytic degradation. (d) All of these problems can be avoided by adding a chemically and electrically inert shell.

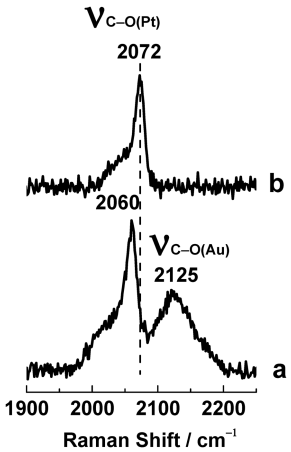

Fig. 3 SERS and SHINERS spectra showing CO adsorption. Bare gold NPs (lower curve) or Au@SiO_2 NPs (upper curve) were spread over a Pt(111) electrode surface, and the electrode was placed in a 0.1 M $HClO_4$ solution saturated with CO gas. Reprinted with permission from *Nature*, 2010, **464**, 392; copyright 2010 Nature Publishing Group.

More importantly, the C–O(Pt) stretching frequency is different in the SERS and SHINERS spectra. It is downshifted to 2060 cm^{-1} in the SERS spectrum because the work functions of these two metals are different (5.1 eV for polycrystalline gold, 5.7 eV for Pt(111)) and charge transfer occurs from gold to platinum.[33] This charge transfer increases electron density at the Pt(111) surface in the vicinity of the gold NPs. On the other hand, SHINERS can provide accurate vibrational information about surface adsorbates. In this case it provides the true C–O(Pt) stretching frequency, 2072 cm^{-1}.

(iii) Contact with probe molecules. A probe molecule adsorbed on the surface of interest may interact with a bare NP as well, adopting a two-end adsorption rather than a one-end adsorption (circled pink/blue molecules in Fig. 2c). This direct contact would change the distribution of electron density in the probe molecule and its adsorption behavior, resulting in significant changes to its SERS spectral features and misleading spectral interpretation. In some cases, a probe molecule may undergo photocatalytic reactions owing to a direct contact between one of its functional groups and the bare NP (exploding yellow/blue molecules in Fig. 2c).

(iv) Stability. Shell-isolated nanoparticles (SHINs) are much more stable than bare NPs because they are coated with an inert shell (Fig. 4).[20] When 10 μL of the concentrated (~1.07 nM) Au@SiO_2 SHIN solution are placed in 0.5 mL of 0.01 M pyridine, the SHINs are stable beyond 240 hours. When 10 μL of the concentrated (~1.07 nM) bare gold NP solution are placed in 0.5 mL of 0.01 M pyridine, the solution changes color in just 3 minutes and shows complete aggregation after 15 minutes.

SHINERS, with its unique shell-isolated mode, can be used to overcome the four problems outlined above. An ultrathin, chemically and electrically inert shell prevents contact with the chemical environment, contact with the surface of interest, and contact with probe molecules (Fig. 2d). If an appropriate shell material is chosen, inadvertent adsorption, charge transfer and photocatalytic reactions can all be avoided. Furthermore, NP stability is greatly improved.

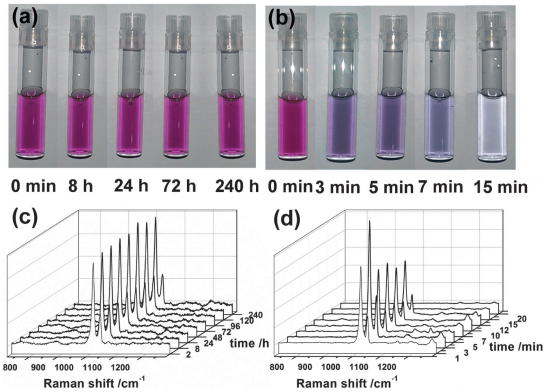

Fig. 4 Comparing the stability of SHINs and bare NPs.[20] Photos of Au@SiO_2 SHINs (a) and bare gold NPs (b) in 0.01 M pyridine solution at different times. Corresponding spectra of pyridine obtained with the SHINs (c) and the bare NPs (d). Reprinted with permission from *Nat. Protoc.*, 2013, **8**, 52; copyright 2013 Nature Publishing Group.

3. 3D-FDTD simulations

Theoretical simulations were carried out using the 3-dimensional finite-difference time-domain (3D-FDTD) method so that electric field distribution could be visualized and Raman scattering enhancement factors could be calculated.[34] Results obtained for a 2 × 2 array of Au@SiO_2 NPs on a perfectly smooth gold surface are presented in Fig. 5. As the gold cores are brought near the smooth gold surface by decreasing shell thickness, localized surface plasmons are excited in the core-to-surface gaps. Electric field is concentrated there, and Raman scattering from molecules adsorbed on the smooth gold surface will increase dramatically. The calculations reveal that electric field strength is enhanced 85 times for the 4 nm shell and 142 times for the 2 nm shell, and that the Raman scattering enhancement factors in the SHIN-to-surface junctions will be 5×10^7 and 4×10^8 for these two shell thicknesses respectively.[19] The calculations also show that the interparticle distance does not significantly affect these values. If the 2 × 2 array is replaced by a single 55 nm Au@4 nm SiO_2 SHIN, electric field strength is enhanced 55 times instead of 85 times and the Raman scattering enhancement factor will be 9×10^6 instead of 5×10^7. It is therefore possible to characterize the adsorption of a monolayer

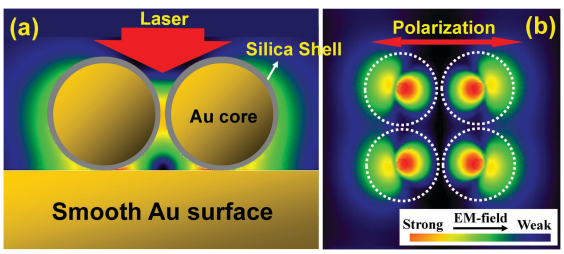

Fig. 5 A 3D-FDTD simulation reveals the distribution of optical electric field surrounding a 2 × 2 array of 55 nm Au@4 nm SiO_2 SHINs on a perfectly smooth gold surface. The shell-to-shell distance is 4 nm. Side view (a) and top view (b); the direction of incidence (a) and the polarization (b) of the 633 nm laser are also shown. Reprinted with permission from *Nature*, 2010, **464**, 392; copyright 2010 Nature Publishing Group.

on an atomically flat single-crystal gold surface, without any interfering signals from the molecule on polycrystalline gold NPs, by SHINERS.

Since the Raman scattering enhancement factor will depend critically on the distance between the gold core and the smooth gold surface, a combined theoretical and experimental investigation into the dependence of Raman intensity on the silica shell thickness was made.[20] The diameter of the gold core was held constant at 55 nm, and pyridine was used as the probe molecule in the experimental component of this study. As expected, Raman intensity decreased exponentially with increasing shell thickness in both the theoretical and the experimental results.

4. Single particle SHINERS

To further understand the surface plasmon physics of SHINERS, several measurements were made on single particles. Fig. 6a shows a dark field microscopy image and a scanning electron microscopy (SEM) image of five individual SHINs on a gold film (120 nm Au@1 nm SiO_2, each circled in red). Fig. 6b provides the surface plasmon resonance (SPR) spectrum of a single SHIN on the gold film. Peak I at 541 nm is assigned to a dipole mode of the particle, and peak II at 608 nm is assigned to a multipolar mode that involves both the particle and the gold film.[35,36] Fig. 6c shows the single particle SHINERS spectrum of pyridine on the gold film.

It is well known that the ~600 nm resonance (peak II) is important for the generation of electromagnetic hot spots in the gap between a particle and a film. If a SHIN is placed on a Si substrate, there is no SPR peak in this region. Then no SHINERS signal can be obtained from pyridine, even if the accumulation time is increased 20-fold. A 514 or 532 nm excitation wavelength, commonly available in Raman systems, cannot be used with a gold particle because so much of this energy is lost to d-sp interband electronic transitions. Hence, the multipolar mode involving the SHIN and the gold film is critical for a large Raman signal enhancement.

5. Various SHIN types

A general overview of the synthetic procedure is provided in Fig. 7.[20] Different SHIN types are used to meet different analysis requirements.

Gold cores with a 55 nm diameter (Fig. 8a) are usually employed because these SHINs are easy to make and provide enough Raman signal enhancement for most applications.[19] Gold cores with a 120 nm diameter (Fig. 8b) are prepared if more enhancement is required.[28] 3D-FDTD simulations have shown that a 120 nm gold core diameter is optimal for use with a 633 nm excitation wavelength. Gold nanocube and nanorod SHINs (Fig. 8c and d) were developed because their SPR absorption maxima can be tuned from the visible to the near infrared by adjusting the nanocube size and nanorod aspect ratio.[20] This quality is essential for biosensor applications. SHINs with a mostly silver core (Fig. 8e) were synthesized because silver is a more efficient plasmonic substrate than gold, and because the SPR of silver nanostructures can be forced to any wavelength in the visible region of the spectrum.[25]

The shell must be less than ~5 nm thick to ensure satisfactory electromagnetic field enhancement. A thicker shell may not allow the desired Raman signal strength. Ultrathin shells consisting of different materials, such as graphene (Fig. 8f and g),[31,32] SiO_2 (Fig. 8h),[19] Al_2O_3 (Fig. 8i)[19] and MnO_2 (Fig. 8j),[24] have been synthesized for specific functions (Sections 9 and 10) and to meet the demands of various chemical environments (*e.g.*, stability in solutions of varying pH).

The most challenging and important part of a SHINERS experiment is the fabrication of an ultrathin shell such that the enhanced electromagnetic field extends from the surface of the core to the surface of interest. Pinholes in the shell become more likely as it is made thinner; and if small areas of the gold core are exposed to the chemical environment through pinholes in the shell, comparably strong SERS signals from molecules on the gold core may interfere with the desired SHINERS signals from molecules on the surface of interest. In general, the shell must be ultrathin, uniform, and free of pinholes for the application of SHINERS to a wide range of chemical systems.

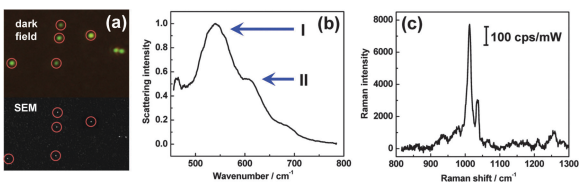

Fig. 6 Dark field and SEM images of individual SHINs on a gold film (a), the SPR spectrum of a single SHIN on the gold film (b), and a single particle SHINERS spectrum of pyridine on the gold film (c). Reprinted with permission from *J. Raman Spectrosc.*, 2013, **44**, 994; copyright 2013 Wiley.

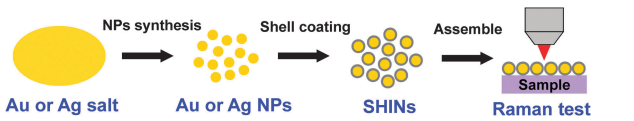

Fig. 7 Overview of SHIN synthesis.

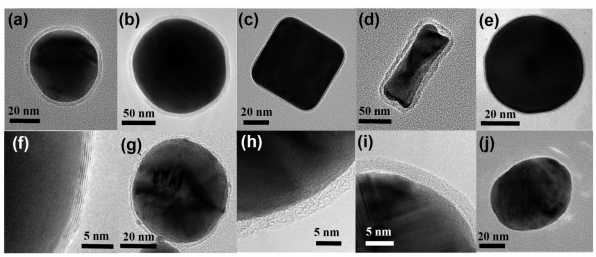

Fig. 8 HR-TEM images of various SHIN types. Au@SiO_2 NPs with a 55 nm spherical core (a), a 120 nm spherical core (b), a nanocube core (c), and a nanorod core (d). A Ag@SiO_2 NP (e) and a Cu@graphene NP (f). SHINs with a core of gold and a shell of graphene (g), SiO_2 (h), Al_2O_3 (i), and MnO_2 (j). f reprinted with permission from *J. Phys. Chem. C*, 2014, **118**, 8993; copyright 2014 American Chemical Society. g reprinted with permission from *Sci. Rep.*, 2014, **4**, 6093; copyright 2014 Nature Publishing Group.

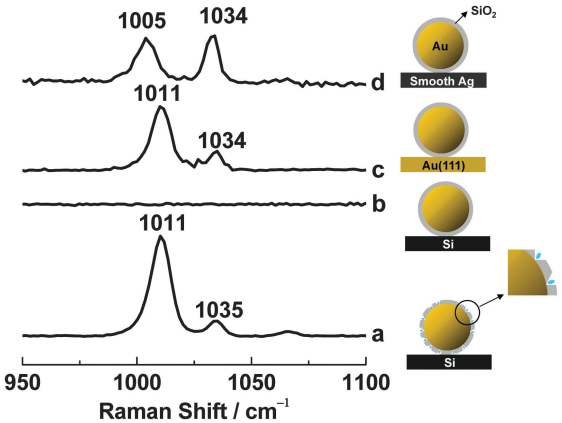

Fig. 9 SHINERS spectra of pyridine using SHINs with pinholes (a) and without pinholes (b) on a Si wafer, without pinholes on a Au(111) single-crystal electrode (c), and without pinholes on a smooth silver electrode (d). Pyridine is adsorbed on gold and silver, but not on Si or silica. a–c reprinted with permission from *Nature*, 2010, **464**, 392; copyright 2010 Nature Publishing Group.

Three methods can be used to ensure that the shell is pinhole-free.[19] First, shell uniformity can be evaluated by high-resolution transmission electron microscopy (HR-TEM). Second, cyclic voltammetry can be used to look for a characteristic gold reduction peak in H_2SO_4 solution. This peak will be absent if the gold cores are isolated by silica shells. Finally, SERS from pyridine on gold will be seen if a small number of pinholes are present in the shell, as pyridine adsorbs on gold but not on silica (Fig. 9).

To demonstrate the last of these tests, 10 μL of a solution containing SHINs with pinholes were placed on a Si wafer and allowed to dry. 20 μL of 10 mM pyridine were added, and a quartz coverslip was placed on top. As expected, strong Raman signals from pyridine adsorbed on the gold cores through the pinholes were seen at 1011 and 1035 cm^{-1} (Fig. 9a). When the procedure was repeated with pinhole-free SHINs, pyridine bands were not observed for several hours (Fig. 9b). When pinhole-free SHINs were instead placed on a Au(111) single-crystal electrode surface, strong Raman peaks were again seen at 1011 and 1034 cm^{-1} (Fig. 9c). In this case, the signals should come from pyridine adsorbed on the Au(111) surface but not from pyridine adsorbed on the gold cores. To further test this, pinhole-free SHINs were dispersed on a smooth silver electrode surface. Two strong Raman peaks with roughly equal intensities were observed, one at 1005 cm^{-1} and the other at 1034 cm^{-1} (Fig. 9d). This is the SERS spectrum of pyridine on silver.[37] All of these results are consistent with pyridine adsorption on the gold core when pinholes are present, but not when pinholes are absent.

Finally, one should be aware that pinholes in the shell are acceptable if the probe molecule does not adsorb on the core material (*e.g.*, hydrogen does not adsorb on gold).

6. Single-crystal electrode surface applications

A free-electron metal must be rough at the nanoscale in order to support surface plasmon activity and give SERS. It is therefore quite difficult to unambiguously characterize adsorption on atomically flat single-crystal surfaces by this method, but the ability to do so would be a great asset in the fields of surface science, electrochemistry and catalysis where single-crystals serve as model systems. It may also provide opportunities to study the SERS selection rule.

SHINERS was introduced to solve this problem, and it was recently used to characterize pyridine adsorption on Au(*hkl*) single-crystal electrode surfaces in an electrochemical environment.[29] The cyclic voltammograms (CVs) in Fig. 10a provide electrochemical points of reference for the SHINERS data in Fig. 10c and d. Fig. 10b gives some typical SHINERS spectra of pyridine on a Au(*hkl*) surface; specifically, Au(111) in the −0.8 to 0.4 V potential range. Large signal/noise ratios are seen. The peaks at 1011 and 1035 cm^{-1} are assigned to the ν_1 ring breathing mode and the ν_{12} symmetric triangular ring deformation mode of the pyridine molecule respectively.[37]

The ν_1 mode frequency is plotted against potential in Fig. 10c. For Au(111), the frequencies (black squares connected by straight lines) change little in the negative potential region and then increase with a Stark tuning rate of 5.6 $cm^{-1}\,V^{-1}$ when $E \geq 0.1$ V. The transition marks a change in the orientation of adsorbed pyridine. The ν_1 frequencies are relatively small at low potentials because pyridine is flat-adsorbed and the binding interaction between π-orbital electrons and the metal is weak. On the other hand, they are relatively large at high potentials because pyridine is vertically adsorbed and the interaction between the nitrogen atom lone-pair electrons and the metal is strong. This result is in agreement with the proposal, based on an extensive analysis of chronocoulometric data made previously by Stolberg *et al.*,[38] that the coverage potential dependence (bold black curve in Fig. 10c) shows pyridine forms a full monolayer on Au(111) at higher potentials.

Pyridine also changes orientation, from flat-adsorbed at low potentials to vertically adsorbed at high potentials, when on Au(100) and Au(110) (red circles and blue triangles in Fig. 10c). The potentials for the completion of a pyridine monolayer increase in the following order: Au(110) < Au(100) < Au(111). This trend follows the potential of the zero charge (E_{pzc}) sequence obtained in the absence of pyridine, 0.06 V for Au(110) < 0.19 V for Au(100) < 0.33 V for Au(111), and suggests that the electrode charge plays a key role in the adsorption process. In addition, ν_1 mode frequencies for the three Au(*hkl*) facets increase in magnitude at a given potential when $E \geq -0.1$ V in the following order: Au(111) < Au(100) < Au(110). This order also coincides with the sequence of E_{pzc} values. It suggests that the binding interaction between pyridine and Au(*hkl*) is affected by surface charge and becomes stronger in the order: Au(111) < Au(100) < Au(110).

It may be seen in Fig. 10d that the ν_1 mode peak intensity for adsorbed pyridine increases as Au(111) < Au(100) ≪ Au(110). The Raman enhancement factors amount to 8.6×10^4 at 0.6 V for Au(111), 2.6×10^5 at 0.3 V for Au(100) and 1.2×10^6 at 0.2 V for Au(110). The same qualitative trend in SHINERS intensity was observed for pyridine on the low-index Pt(*hkl*) surfaces.[22] Density functional theory (DFT) calculations and a theoretical

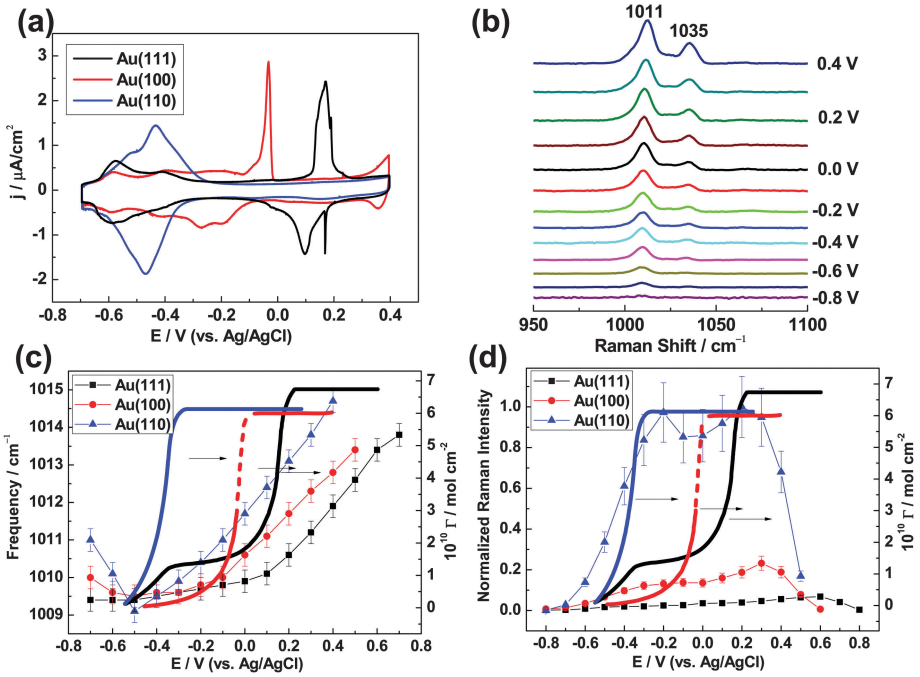

Fig. 10 (a) CVs obtained from Au(111), Au(100) and Au(110) electrodes in 1 mM pyridine + 0.1 M $NaClO_4$ using a Pt coil auxiliary electrode and a Ag/AgCl reference electrode. (b) SHINERS spectra of pyridine on a Au@SiO_2 NP film Au(111) electrode in the potential range −0.8 to 0.4 V. The dependence of Raman frequency (c) and normalized Raman intensity (d) on applied potential for the pyridine ν_1 ring breathing mode (data points connected by straight lines), and these are compared with surface concentration isotherms (bold curves). Reprinted with permission from *J. Am. Chem. Soc.*, 2015, **137**, 2400; copyright 2015 American Chemical Society.

analysis of dielectric functions indicate that this facet dependence of SHINERS intensity is for the most part governed by the dielectric properties of the single-crystals, which result in different SHIN-to-surface electromagnetic field coupling strengths.[22]

Thus, SHINERS can be used to characterize metal–molecule interactions which are difficult or impossible to characterize by more traditional methods, such as pyridine adsorption on Au(*hkl*) single-crystal electrode surfaces. It can be used to understand the correlations that exist between the structure and reactivity for a wide range of interfacial phenomena.

7. Food inspection

The accurate and rapid detection of pesticides on food can be accomplished by SHINERS using a portable Raman spectrometer. This agricultural and industrial application is demonstrated in Fig. 11.

The ordinary Raman spectrum of a clean orange skin (Fig. 11a) and the ordinary Raman spectrum of an orange skin contaminated with parathion pesticide (Fig. 11b) are essentially the same. The bands at 1165 and 1526 cm^{-1} are due to naturally occurring carotenoids. SHINs with a 20 by 60 nm gold nanorod core, for resonance with a 785 nm excitation wavelength, and a 2 nm silica shell were then added to the contaminated orange skin. Parathion bands[39] appear at 1109 and 1339 cm^{-1} (Fig. 11c).

Furthermore, the simultaneous detection of multiple pesticides can be accomplished with SHINERS. Fig. 11d and e show typical SHINERS spectra of cabbage leaves contaminated with

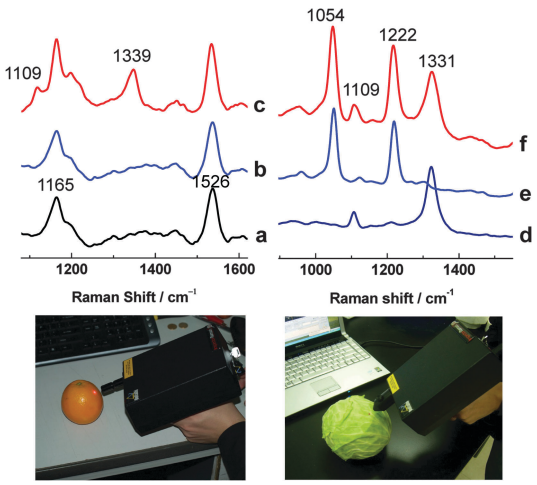

Fig. 11 Testing for pesticide residues using a DeltaNu Inspector Raman spectrometer (785 nm excitation, 30 mW on the sample, 30 second accumulation). Ordinary Raman spectra were obtained from an orange skin before (a) and after (b) it was sprayed with parathion. A SHINERS spectrum was then obtained from the contaminated orange skin (c). SHINERS spectra were acquired from a cabbage after it was sprayed with parathion (d), fenthion (e), and both of these pesticides (f). a–c reprinted with permission from *Nature*, 2010, **464**, 392; copyright 2010 Nature Publishing Group.

parathion and fenthion pesticides respectively. Fig. 11f shows that both pesticides can be detected at the same time. Parathion bands[39] are seen at 1109 and 1331 cm^{-1}, and fenthion bands[40] appear at 1054 and 1222 cm^{-1}. These results demonstrate

SHINERS' tremendous potential as a field-portable method of analysis for agricultural and industrial inspection applications.

8. Cultural heritage science

Raman spectroscopy is commonly used to analyze objects of cultural importance. Ordinary Raman scattering is intrinsically weak, however, and the fluorescence of resonant dyes can make their Raman signals even more difficult to obtain. The importance of SERS in this field has grown quickly in recent years because of the sensitivity increase and fluorescence quenching that it offers.[41–43] Yet this method has its own challenges. When the analyte is placed in contact with a SERS substrate of gold or silver, charge transfer can result in changes to the spectrum of the unknown.[44,45] Then a SERS-specific library of reference spectra may be required for compound identification. A SERS library must be specific for the metal used, since gold and silver yield different charge transfer effects. Changes in the spectrum of the analyte also depend on its orientation relative to the metal, and multiple reference spectra may be required for a single molecule/metal combination. A chemically inert shell around the metal will prevent charge transfer; and if it is sufficiently thin, it will permit the enhanced electromagnetic field to reach the analyte. It will also permit fluorescence quenching if it is just a few nanometers thick.[46]

In this section, it is shown that an inert shell can eliminate the need for a SERS-specific library. Historically, thiazine dyes have been used on paper, textiles and leather.[47] They are of interest here because they can interact with gold in a variety of ways: through a conjugated π system, through a hetero atom lone pair of electrons, and through an amine lone pair. Thionine (color index number CI 52000, also called Lauth's violet) is the structurally simplest thiazine dye, and the one chosen for this proof of concept.

Ordinary Raman spectra were collected from solid crystals of thionine, SERS spectra were collected from thionine adsorbed on bare gold NPs with a 55 nm diameter, and SHINERS spectra were collected from thionine adsorbed on NPs with a 55 nm gold core and a 3 to 4 nm silica shell. Samples were prepared for SERS and SHINERS analysis by placing a drop of the appropriate NP solution on separate glass microscope slides and allowing the aqueous solvent to evaporate. Each slide was then held at an angle while 50 μL of 10 μM thionine in methanol were added to the slide above the NPs and allowed to run over top. Excess dye was wicked away from the bottom of each slide with a piece of laboratory tissue, and the remaining solvent was allowed to evaporate. Water was placed on the surface of each slide, allowed to remain in contact with the thionine-covered NPs for a couple of seconds, then poured off. The goal of this procedure was to cover the NPs with as close to a monolayer of the dye as possible so that a strong effect can be observed.

The results are presented in Fig. 12. A number of changes appear between the ordinary Raman spectrum (Fig. 12a) and the bare gold NP SERS spectrum (Fig. 12b), then disappear in the gold-core silica-shell NP SHINERS spectrum (Fig. 12c). First,

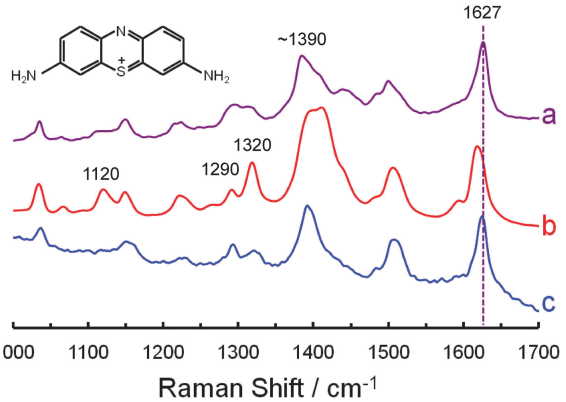

Fig. 12 The structure of thionine (inset). Ordinary Raman spectrum of thionine powder (a) obtained with a 0.02 mW laser power and a 60 second accumulation time. Bare gold NP SERS (b) and gold-core silica-shell NP SHINERS (c) spectra of adsorbed thionine obtained with a 1 mW laser power and a 300 second accumulation time. All three spectra were collected with a Bruker Senterra Raman microscope employing the 633 nm He–Ne laser line. They were normalized to the height of the 1627 cm^{-1} peak and offset for clarity.

the 1627 cm^{-1} band in the ordinary Raman spectrum shifts to 1619 cm^{-1} in the SERS spectrum and then shifts back to 1625 cm^{-1} in the SHINERS spectrum. A vertical, dashed violet line appears in the figure to highlight these changes. Second, the overall shape of the 1350 to 1450 cm^{-1} region is similar in the ordinary Raman and SHINERS spectra, but different in the SERS spectrum. Third, the intensity of the 1290 cm^{-1} band is greater than the intensity of the 1320 cm^{-1} band in the ordinary Raman spectrum, the relative heights of these peaks are reversed in the SERS spectrum, then they are reversed again in the SHINERS spectrum. Fourth, the intensity of the 1120 cm^{-1} band is relatively low in the ordinary Raman spectrum, increases in the SERS spectrum, and decreases again in the SHINERS spectrum.

Fig. 12 shows that an inert shell can eliminate the need for a SERS-specific library. The NPs remain effective even after they have been stored for some time, as the spectra in Fig. 12b and c were obtained using 4 month old NPs and they are similar to spectra obtained using 1 week old NPs. Thionine does not absorb at the laser wavelength used here, but the fluorescence of resonant dyes was indeed quenched in SHINERS experiments (fluorescence quenching will be detailed in later publications). It is worth noting that silica shells can also be applied to silver NPs[25] because silver is more commonly used than gold in conservation science. Further work, directed toward applying this methodology to the analysis of heritage objects, is currently underway at the Canadian Conservation Institute.

9. Multimodal cell imaging with GIANs

Graphene can offer special advantages as a nanoparticle isolating material.[32,48,49] First, it provides strong D and G vibrational mode SERS signals at around 1325 and 1595 cm^{-1}, as shown in Fig. 13a. Either of these bands can be used for Raman imaging. Second, graphene-isolated Au nanoparticles (GIANs)

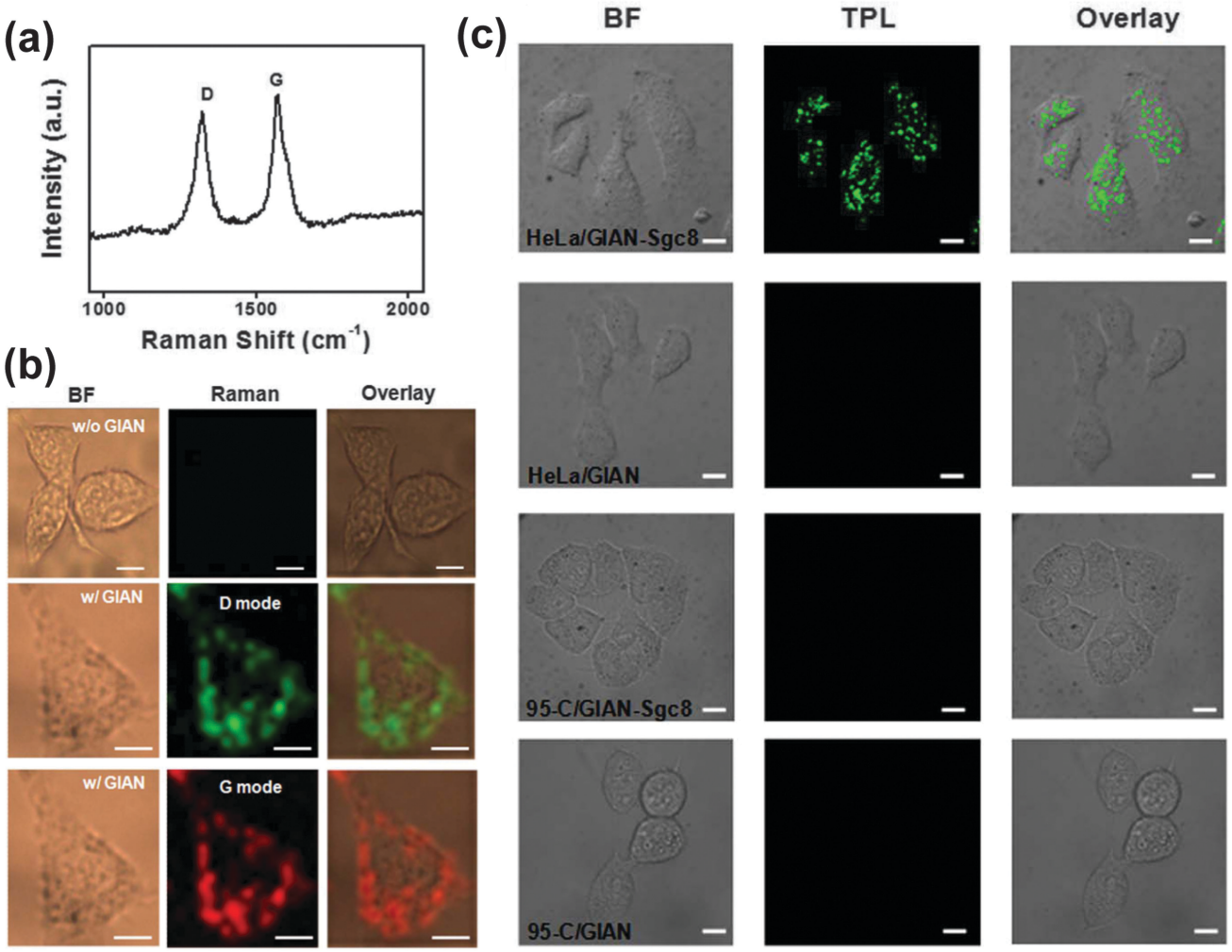

Fig. 13 Multimodal cell imaging with GIANs. (a) The Raman spectrum of GIANs (633 nm excitation). (b) Bright field images of MCF-7 cells, and Raman images obtained by monitoring the D and G modes shown in a. (c) Bright field images of HeLa cells and 95-C cells incubated with GIAN and GIAN-Sgc8, and two-photon luminescence images demonstrating cell selectivity. Reprinted with permission from *Sci. Rep.*, 2014, **4**, 6093; copyright 2014 Nature Publishing Group.

may be functionalized through hydrophobic interactions, which are thermodynamic in nature, or π bonding.[2] For example, they can be made water soluble by the addition of polyoxyethylene stearyl ether (PEG) molecules when the hydrophobic alkyl chains anchor to the hydrophobic GIAN surface. Third, GIANs are biocompatible. GIANs that have been made water soluble by the addition of PEG are endocytosed by living cells.

Bright field images of MCF-7 breast cancer cells are presented in the first column of Fig. 13b. Raman images, obtained by monitoring the D and G vibrational modes, are presented in the second column. It may be seen from the overlaid images in the third column that GIANs are distributed throughout the cytoplasm, with no Raman signal arising from the nucleus of the cell.

Furthermore, GIANs exhibit two-photon luminescence (TPL). The advantages of TPL imaging include minimal autofluorescence background, minimal photon-induced damage to the sample, and high spatial resolution. Because a near infrared wavelength in the optically transparent window for biological samples is normally used to excite TPL, increased light penetration is also accomplished. If the graphene shell is functionalized with an aptamer that interacts preferentially with a certain type of cell, targeted cell imaging can be achieved. This is shown in Fig. 13c. Sgc8 aptamers bind selectively to protein tyrosine kinase 7 (PTK7) cell membrane proteins. They adsorb on graphene through π–π interactions, and show a higher binding affinity for HeLa cervical cancer cells than for 95-C lung cancer cells. Therefore, HeLa cells could be imaged by GIAN TPL whereas 95-C cells remained dark. It is believed that SPR of the gold core and two-photon absorption by the graphene shell both contribute to the TPL signal, as bare gold NPs and hollow carbon capsules both exhibit the TPL effect.

10. Photothermal cancer therapy and photothermally-enhanced chemotherapy with GIANs

GIANs have shown great potential in photothermal cancer therapy and photothermally-enhanced chemotherapy.[32] The former entails placement of GIANs in a sample of cancer cells and irradiating with near infrared laser light. GIANs strongly absorb in the near infrared

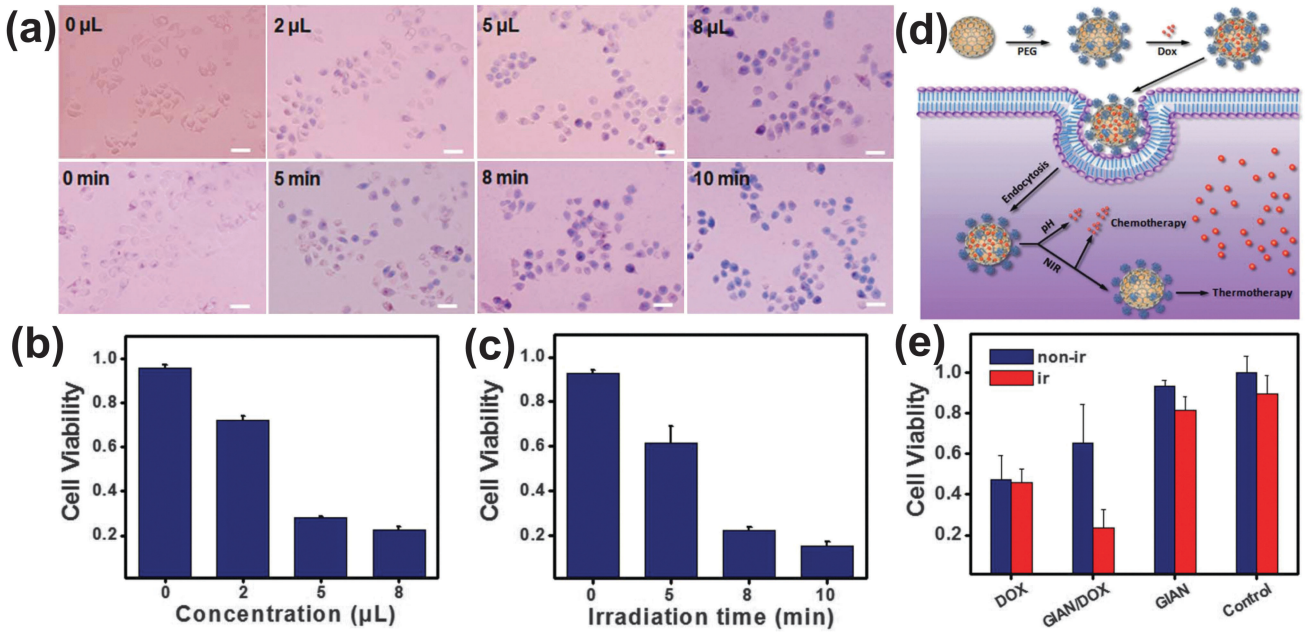

Fig. 14 Cancer therapy with GIANs. (a) Bright field images of MCF-7 cells after treatment with varying amounts of 0.2 mg mL^{-1} GIAN solution (constant irradiation time), and varying irradiation times with an 808 nm laser at 2 W cm^{-2} (constant amount of GIAN solution). Trypan blue was used to stain dead cells. The scale bar represents 50 μm. (b and c) Cell viability after treatment with varying amounts of GIAN solution and varying irradiation times. (d) Schematic overview: GIANS are functionalized with Dox, they are endocytosed, the anticancer drug is released, and GIANs continue to facilitate photothermal cancer therapy. (e) MCF-7 cell viability after treatment with free Dox, GIANs loaded with Dox, and GIANs never loaded with Dox. All three of these treatments were tested without and with 808 nm laser irradiation. Reprinted with permission from *Sci. Rep.*, 2014, **4**, 6093; copyright 2014 Nature Publishing Group.

region of the spectrum, so they can rapidly increase the temperature of their surroundings and cause cell death. In the latter, this effect is combined with release of an anticancer drug.

Fig. 14a shows MCF-7 breast cancer cells which can be stained with trypan blue only after death. The photothermal treatment is made more effective by increasing the amount of 0.2 mg mL^{-1} GIAN solution added (constant irradiation time), and increasing the irradiation time with an 808 nm laser at 2 W cm^{-2} (a constant amount of GIAN solution). Fig. 14b and c show that more than 80% of the cells died with the addition of 8 μL of the GIAN solution and 8 minutes of laser irradiation.

In a separate set of experiments, GIANs were functionalized with the anticancer drug doxorubicin (Dox) through π bonding. Following endocytosis by MCF-7 cells, a relatively slow partial release of Dox was caused by the low pH inside the endosome, and a further controlled release was accomplished by heating the GIANs *via* near infrared laser irradiation (Fig. 14d). After release of the Dox, GIANs continued to facilitate photothermal cancer therapy. Cell viabilities are compared in Fig. 14e. In the absence of laser irradiation, treatment with free Dox was found to be most effective. With laser irradiation, however, the combination of GIAN-mediated Dox delivery and photothermal cancer therapy was proved to be significantly more effective than treatment with free Dox.

11. Conclusion and perspectives

By replacing the direct contact mode (SERS) or the non-contact mode (TERS) with the shell-isolated one, SHINERS has mostly broken the long-standing material-specific and morphology-specific limitations of SERS. SHINERS has made it possible to detect, identify and characterize various analytes and materials that were either very difficult to examine or completely inaccessible before. In this Tutorial Review we have shown that it can be used to characterize adsorption on single-crystal electrode surfaces, detect pesticides on food using a field-portable Raman spectrometer, eliminate charge transfer effects for the identification of unknown dyes in cultural heritage science, carry out multimodal cell imaging, and destroy cancer cells *in vitro*.

Since the shell can be used to attenuate hot-electron transfer from the core to a molecule or metal, SHINERS can offer new possibilities for the study of photocatalytic reactions and the development of metal–insulator–metal (MIM) device architectures. In the Tian and Li groups, the concept of the SHIN enhancement is being applied to other spectroscopies such as infrared absorption and sum frequency generation. Aroca and co-workers have applied it to fluorescence.[50]

As a method of analysis, SHINERS is fast, inexpensive, simple and reliable. Beyond that, the shell-isolated mode is extremely flexible and of use in many areas of science and technology.

Acknowledgements

We thank Zhong-Lin Wang, Zhi-Lin Yang, Wei-Hong Tan, Jin Zhang and Jennifer Poulin for helpful discussions. J. F. L. and Z. Q. T. thank the NSFC (21522508 and 21427813), MOST of

China (2011YQ030124 and 2015CB932301), and the Thousand Youth Talents Plan of China for support.

References

1 *Surface Enhanced Raman Scattering*, ed. R. K. Chang and T. E. Furtak, Plenum Press, New York, 1982.
2 R. L. McCreery, *Raman Spectroscopy for Chemical Analysis*, John Wiley, New York, 2000.
3 *Surface-Enhanced Raman Scattering Physics and Applications*, ed. K. Kneipp, M. Moskovits and H. Kneipp, Springer, Berlin/Heidelberg, 2006.
4 E. C. Le Ru and P. G. Etchegoin, *Principles of Surface-Enhanced Raman Spectroscopy and Related Plasmonic Effects*, Elsevier, Amsterdam/Oxford, 2009.
5 *Frontiers of Surface-Enhanced Raman Scattering: Single Nanoparticles and Single Cells*, ed. Y. Ozaki, K. Kneipp and R. Aroca, Wiley, Chichester, 2014.
6 S. M. Nie and S. R. Emory, *Science*, 1997, **275**, 1102–1106.
7 K. Kneipp, Y. Wang, H. Kneipp, L. T. Perelman, I. Itzkan, R. Dasari and M. S. Feld, *Phys. Rev. Lett.*, 1997, **78**, 1667–1670.
8 M. Moskovits, *Rev. Mod. Phys.*, 1985, **57**, 783–826.
9 J. P. Camden, J. A. Dieringer, J. Zhao and R. P. Van Duyne, *Acc. Chem. Res.*, 2008, **41**, 1653–1661.
10 J. J. Baumberg, T. A. Kelf, Y. Sugawara, S. Cintra, M. E. Abdelsalam, P. N. Bartlett and A. E. Russell, *Nano Lett.*, 2005, **5**, 2262–2267.
11 W. L. Barnes, A. Dereux and T. W. Ebbesen, *Nature*, 2003, **424**, 824–830.
12 S. Lal, N. K. Grady, J. Kundu, C. S. Levin, J. B. Lassiter and N. J. Halas, *Chem. Soc. Rev.*, 2008, **37**, 898–911.
13 D. Graham, D. G. Thompson, W. E. Smith and K. Faulds, *Nat. Nanotechnol.*, 2008, **3**, 548–551.
14 M. J. Banholzer, J. E. Millstone, L. D. Qin and C. A. Mirkin, *Chem. Soc. Rev.*, 2008, **37**, 885–897.
15 L. Tong, T. Zhu and Z. Liu, *Chem. Soc. Rev.*, 2011, **40**, 1296–1304.
16 M. Moskovits, *J. Raman Spectrosc.*, 2005, **36**, 485–496.
17 R. M. Stockle, Y. D. Suh, V. Deckert and R. Zenobi, *Chem. Phys. Lett.*, 2000, **318**, 131–136.
18 B. Pettinger, B. Ren, G. Picardi, R. Schuster and G. Ertl, *Phys. Rev. Lett.*, 2004, **92**, 096101.
19 J. F. Li, Y. F. Huang, Y. Ding, Z. L. Yang, S. B. Li, X. S. Zhou, F. R. Fan, W. Zhang, Z. Y. Zhou, D. Y. Wu, B. Ren, Z. L. Wang and Z. Q. Tian, *Nature*, 2010, **464**, 392–395.
20 J. F. Li, X. D. Tian, S. B. Li, J. R. Anema, Z. L. Yang, Y. Ding, Y. F. Wu, Y. M. Zeng, Q. Z. Chen, B. Ren, Z. L. Wang and Z. Q. Tian, *Nat. Protoc.*, 2013, **8**, 52–65.
21 J. R. Anema, J. F. Li, Z. L. Yang, B. Ren and Z. Q. Tian, *Annu. Rev. Anal. Chem.*, 2011, **4**, 129–150.
22 J. F. Li, S. Y. Ding, Z. L. Yang, M. L. Bai, J. R. Anema, X. Wang, A. Wang, D. Y. Wu, B. Ren, S. M. Hou, T. Wandlowski and Z. Q. Tian, *J. Am. Chem. Soc.*, 2011, **133**, 15922–15925.
23 D. P. Butcher, S. P. Boulos, C. J. Murphy, R. C. Ambrosio and A. A. Gewirth, *J. Phys. Chem. C*, 2012, **116**, 5128–5140.
24 X. D. Lin, V. Uzayisenga, J. F. Li, P. P. Fang, D. Y. Wu, B. Ren and Z. Q. Tian, *J. Raman Spectrosc.*, 2012, **43**, 40–45.
25 V. Uzayisenga, X. D. Lin, L. M. Li, J. R. Anema, Z. L. Yang, Y. F. Huang, H. X. Lin, S. B. Li, J. F. Li and Z. Q. Tian, *Langmuir*, 2012, **28**, 9140–9146.
26 L. Lin, X. D. Tian, S. L. Hong, P. Dai, Q. C. You, R. Y. Wang, L. S. Feng, C. Xie, Z. Q. Tian and X. Chen, *Angew. Chem., Int. Ed.*, 2013, **52**, 7266–7271.
27 A. Tittl, X. H. Yin, H. Giessen, X. D. Tian, Z. Q. Tian, C. Kremers, D. N. Chigrin and N. Liu, *Nano Lett.*, 2013, **13**, 1816–1821.
28 X. D. Tian, B. J. Liu, J. F. Li, Z. L. Yang, B. Ren and Z. Q. Tian, *J. Raman Spectrosc.*, 2013, **44**, 994–998.
29 J. F. Li, Y. J. Zhang, A. V. Rudnev, J. R. Anema, S. B. Li, W. J. Hong, P. Rajapandiyan, J. Lipkowski, T. Wandlowski and Z. Q. Tian, *J. Am. Chem. Soc.*, 2015, **137**, 2400–2408.
30 D. Graham, *Angew. Chem., Int. Ed.*, 2010, **49**, 9325–9327.
31 Y. M. Liu, Y. Hu and J. Zhang, *J. Phys. Chem. C*, 2014, **118**, 8993–8998.
32 X. Bian, Z. L. Song, Y. Qian, W. Gao, Z. Q. Cheng, L. Chen, H. Liang, D. Ding, X. K. Nie, Z. Chen and W. H. Tan, *Sci. Rep.*, 2014, **4**, 6093.
33 J. A. Rodriguez and D. W. Goodman, *Science*, 1992, **257**, 897–903.
34 K. S. Kunz and R. J. Luebbers, *The finite difference time domain method for electromagnetics*, CRC Press, Boca Raton, FL, 1993.
35 N. J. Halas, S. Lal, W. S. Chang, S. Link and P. Nordlander, *Chem. Rev.*, 2011, **111**, 3913–3961.
36 D. K. Gramotnev and S. I. Bozhevolnyi, *Nat. Photonics*, 2010, **4**, 83–91.
37 D. Y. Wu, J. F. Li, B. Ren and Z. Q. Tian, *Chem. Soc. Rev.*, 2008, **37**, 1025–1041.
38 L. Stolberg, S. Morin, J. Lipkowski and D. E. Irish, *J. Electroanal. Chem.*, 1991, **307**, 241–242.
39 D. Lee, S. Lee, G. H. Seong, J. Choo, E. K. Lee and D. G. Gweon, *Appl. Spectrosc.*, 2006, **60**, 373–377.
40 S. G. Skoulika, C. A. Georgiou and M. G. Polissiou, *Appl. Spectrosc.*, 1999, **53**, 1470–1474.
41 F. Casadio, M. Leona, J. R. Lombardi and R. Van Duyne, *Acc. Chem. Res.*, 2010, **43**, 782–791.
42 K. L. Wustholz, C. L. Brosseau, F. Casadio and R. P. Van Duyne, *Phys. Chem. Chem. Phys.*, 2009, **11**, 7350–7359.
43 K. Chen, M. Leona and T. Vo-Dinh, *Sens. Rev.*, 2007, **27**, 109–120.
44 A. Otto, I. Mrozek, H. Grabhorn and W. Akemann, *J. Phys.: Condens. Matter*, 1992, **4**, 1143–1212.
45 F. Pozzi, S. Porcinai, J. R. Lombardi and M. Leona, *Anal. Methods*, 2013, **5**, 4205–4212.
46 S. Saini, H. Singh and B. Bagchi, *J. Chem. Sci.*, 2006, **118**, 23–35.
47 H. Berneth, *"Azine Dyes" in Ullmann's Encyclopedia of Industrial Chemistry*, Wiley-VCH Verlag GmbH & Co. KGaA, 2008.
48 H. Liang, X. B. Zhang, Y. F. Lv, L. Gong, R. W. Wang, X. Y. Zhu, R. H. Yang and W. H. Tan, *Acc. Chem. Res.*, 2014, **47**, 1891–1901.
49 W. G. Xu, N. N. Mao and J. Zhang, *Small*, 2013, **9**, 1206–1224.
50 A. R. Guerrero and R. F. Aroca, *Angew. Chem., Int. Ed.*, 2011, **50**, 665–668.